REPORT DOCUMENTATION PAGE

Form Approved OMB NO. 0704-0188

The public reporting burden for this collection of information is estimated to average 1 hour per response, including the time for reviewing instructions, searching existing data sources, gathering and maintaining the data needed, and completing and reviewing the collection of information. Send comments regarding this burden estimate or any other aspect of this collection of information, including suggesstions for reducing this burden, to Washington Headquarters Services, Directorate for Information Operations and Reports, 1215 Jefferson Davis Highway, Suite 1204, Arlington VA, 22202-4302. Respondents should be aware that notwithstanding any other provision of law, no person shall be subject to any oenalty for failing to comply with a collection of information if it does not display a currently valid OMB control number.
PLEASE DO NOT RETURN YOUR FORM TO THE ABOVE ADDRESS.

1. REPORT DATE (DD-MM-YYYY) 31-12-2013	2. REPORT TYPE Final Report	3. DATES COVERED (From - To) 1-Oct-2009 - 31-Dec-2011

4. TITLE AND SUBTITLE Collaborative Research: Effects of Stability, Canopies, and Non-Stationarity on Dispersion in the Stable Boundary Layer	5a. CONTRACT NUMBER W911NF-09-1-0572
	5b. GRANT NUMBER
	5c. PROGRAM ELEMENT NUMBER 611102
6. AUTHORS Jeffrey C. Weil, Edward G. Patton, Peter P. Sullivan	5d. PROJECT NUMBER
	5e. TASK NUMBER
	5f. WORK UNIT NUMBER

7. PERFORMING ORGANIZATION NAMES AND ADDRESSES University of Colorado - Boulder 3100 Marine Street, Room 479 572 UCB Boulder, CO 80303 -1058	8. PERFORMING ORGANIZATION REPORT NUMBER

9. SPONSORING/MONITORING AGENCY NAME(S) AND ADDRESS (ES) U.S. Army Research Office P.O. Box 12211 Research Triangle Park, NC 27709-2211	10. SPONSOR/MONITOR'S ACRONYM(S) ARO
	11. SPONSOR/MONITOR'S REPORT NUMBER(S) 56258-EV.12

12. DISTRIBUTION AVAILIBILITY STATEMENT

Approved for Public Release; Distribution Unlimited

13. SUPPLEMENTARY NOTES
The views, opinions and/or findings contained in this report are those of the author(s) and should not contrued as an official Department of the Army position, policy or decision, unless so designated by other documentation.

14. ABSTRACT

Under previous support from the Army Research Office (ARO), we developed Lagrangian particle dispersion models (LPDMs) for dispersion in convective and stable planetary boundary layers (PBLs) including some with a forest canopy and showed that predicted concentration fields agreed well with laboratory data and field observations. For the ARO program just completed, this work was extended to dispersion

15. SUBJECT TERMS

Turbulence, planetary boundary layer, plant canopies, dispersion, large eddy simulations, Lagrangian particle dispersion model

16. SECURITY CLASSIFICATION OF:			17. LIMITATION OF ABSTRACT	15. NUMBER OF PAGES	19a. NAME OF RESPONSIBLE PERSON Jeffrey Weil
a. REPORT UU	b. ABSTRACT UU	c. THIS PAGE UU	UU		19b. TELEPHONE NUMBER 303-497-8907

Standard Form 298 (Rev 8/98)
Prescribed by ANSI Std. Z39.18

Report Title

Collaborative Research: Effects of Stability, Canopies, and Non-Stationarity on Dispersion in the Stable Boundary Layer

ABSTRACT

Under previous support from the Army Research Office (ARO), we developed Lagrangian particle dispersion models (LPDMs) for dispersion in convective and stable planetary boundary layers (PBLs) including some with a forest canopy and showed that predicted concentration fields agreed well with laboratory data and field observations. For the ARO program just completed, this work was extended to dispersion in more stable PBLs and stable boundary layers (SBLs) over horizontally heterogeneous surfaces. This was pursued in part using our new coupled multi-layer canopy - soil model. The program consisted of three main investigations. The first had two parts: a) further development of the coupled-canopy large-eddy simulation (LES) model and comparison with observations from the CHATS (Canopy Horizontal Array Turbulence Study) field program, and b) modeling of canopy dispersion using the LPDM-LES approach and assessment of this with the CHATS dispersion data. The second was an investigation of the effects of a surface-temperature heterogeneity on dispersion in the SBL. The third study a) used the coupled model to produce a more stable boundary layer and applied the LES fields generated from this to drive our LPDM, and b) developed an LPDM based on parameterized turbulence profiles for modeling dispersion in more stable PBLs.

Enter List of papers submitted or published that acknowledge ARO support from the start of the project to the date of this printing. List the papers, including journal references, in the following categories:

(a) Papers published in peer-reviewed journals (N/A for none)

Received		Paper
05/29/2013	2.00	Sylvain Dupont, Edward G. Patton. Influence of stability and seasonal canopy changes on micrometeorology within and above an orchard canopy: The CHATS experiment, Agricultural and Forest Meteorology, (05 2012): 0. doi: 10.1016/j.agrformet.2012.01.011
05/29/2013	3.00	S. Dupont, E. G. Patton. Momentum and scalar transport within a vegetation canopy following atmospheric stability and seasonal canopy changes: the CHATS experiment, Atmospheric Chemistry and Physics, (07 2012): 0. doi: 10.5194/acp-12-5913-2012
05/29/2013	4.00	S. L. Edburg, D. Stock, B. K. Lamb, E. G. Patton. The Effect of the Vertical Source Distribution on Scalar Statistics within and above a Forest Canopy, Boundary-Layer Meteorology, (12 2011): 0. doi: 10.1007/s10546-011-9686-1
05/29/2013	5.00	Peter P. Sullivan, Edward G. Patton. The Effect of Mesh Resolution on Convective Boundary Layer Statistics and Structures Generated by Large-Eddy Simulation, Journal of the Atmospheric Sciences, (10 2011): 0. doi: 10.1175/JAS-D-10-05010.1

TOTAL: **4**

Number of Papers published in peer-reviewed journals:

(b) Papers published in non-peer-reviewed journals (N/A for none)

Received   Paper

TOTAL:

Number of Papers published in non peer-reviewed journals:

(c) Presentations

Number of Presentations: 0.00

Non Peer-Reviewed Conference Proceeding publications (other than abstracts):

Received   Paper

05/28/2013 6.00 Jeffrey C Weil. Stable boundary layer modeling for air quality applications,
31st NATO/SPS International Technical Meeting on Air Pollution Modeling and its Application. 27-SEP-10,
. : ,

TOTAL: **1**

Number of Non Peer-Reviewed Conference Proceeding publications (other than abstracts):

Peer-Reviewed Conference Proceeding publications (other than abstracts):

Received   Paper

TOTAL:

Number of Peer-Reviewed Conference Proceeding publications (other than abstracts):

(d) Manuscripts

Received		Paper

05/28/2013 1.00 Jeffrey C Weil, Peter P Sullivan, Edward G Patton, Chin-Hoh Moeng. Statistical variability of dispersion in the convective boundary layer: Ensembles of simulations and observations,
Boundary-Layer Meteorology (02 2012)

12/31/2013 11.00 Peter P. Sullivan, Jeffrey C. Weil, Edward G. Patton, Chin-Hoh Moeng. Statistical Variability of Dispersion in the Convective Boundary Layer: Ensembles of Simulations and Observations,
Boundary-Layer Meteorology (03 2012)

12/31/2013 10.00 Eugene J. Allwine, Steven L. Edburg, Brian K. Lamb, Roni Avissar, Ronald J. Calhoun, Jan Kleissl, William J. Massman, Kyaw Tha Paw U, Jeffrey C. Weil, Edward G. Patton, Thomas W. Horst, Peter P. Sullivan, Donald H. Lenschow, Steven P. Oncley, William O. J. Brown, Sean P. Burns, Alex B. Guenther, Andreas Held, Thomas Karl, Shane D. Mayor, Luciana V. Rizzo, Scott M. Spuler, Jielun Sun, Andrew A. Turnipseed. The Canopy Horizontal Array Turbulence Study,
Bulletin of the American Meteorological Society (05 2011)

TOTAL: **3**

Number of Manuscripts:

Books

Received		Paper

05/28/2013 7.00 Jeffrey C. Weil. Atmospheric dispersion, United States: CRC, Taylor and Francis, (12 2012)

05/29/2013 8.00 Edward G. Patton, John J. Finnigan. Canopy Turbulence, United States: CRC, Taylor and Francis, (12 2012)

05/29/2013 9.00 Roger H. Shaw, Edward G. Patton, John J. Finnigan. Coherent eddy structures over plant canopies, United States: Wiley, (09 2013)

TOTAL: **3**

Patents Submitted

Patents Awarded

Awards

Jeffrey Weil received the Distinguished Career Award from the University of Delaware Mechanical Engineering Department in April 2013

Graduate Students

NAME	PERCENT_SUPPORTED
FTE Equivalent:	
Total Number:	

Names of Post Doctorates

NAME	PERCENT_SUPPORTED
FTE Equivalent:	
Total Number:	

Names of Faculty Supported

NAME	PERCENT_SUPPORTED
FTE Equivalent:	
Total Number:	

Names of Under Graduate students supported

NAME	PERCENT_SUPPORTED
FTE Equivalent:	
Total Number:	

Student Metrics
This section only applies to graduating undergraduates supported by this agreement in this reporting period

The number of undergraduates funded by this agreement who graduated during this period: ......

The number of undergraduates funded by this agreement who graduated during this period with a degree in science, mathematics, engineering, or technology fields:......

The number of undergraduates funded by your agreement who graduated during this period and will continue to pursue a graduate or Ph.D. degree in science, mathematics, engineering, or technology fields:......

Number of graduating undergraduates who achieved a 3.5 GPA to 4.0 (4.0 max scale):......

Number of graduating undergraduates funded by a DoD funded Center of Excellence grant for Education, Research and Engineering:......

The number of undergraduates funded by your agreement who graduated during this period and intend to work for the Department of Defense ......

The number of undergraduates funded by your agreement who graduated during this period and will receive scholarships or fellowships for further studies in science, mathematics, engineering or technology fields:......

Names of Personnel receiving masters degrees

NAME
Total Number:

Names of personnel receiving PHDs

NAME

Total Number:

Names of other research staff

NAME   PERCENT_SUPPORTED

FTE Equivalent:
Total Number:

Sub Contractors (DD882)

Inventions (DD882)

Scientific Progress

See attachment.

Technology Transfer

Final Progress Report
Grant/Contract Number: W911NF-09-1-0572

Collaborative Research: Effects of Stability, Canopies, and Non-Stationarity on Dispersion in the Stable Boundary Layer

Jeffrey C. Weil

Cooperative Institute for Research in Environmental Sciences
University of Colorado, Boulder, Colorado

Edward G. Patton and Peter P. Sullivan

Mesoscale and Microscale Meteorology Division
National Center for Atmospheric Research, Boulder, CO

Contents

List of Figures

List of Tables

1. Introduction

Dispersion in the stable boundary layer (SBL) is important for a range of problems including air quality and toxic gas releases, but existing information on SBL dispersion is deficient due to our limited understanding of SBL turbulence. This deficiency is attributed to the weakness of the turbulence and the range of processes complicating the SBL physics. Large-eddy simulation (LES) has proven to be a powerful tool in simulating turbulence in the planetary boundary layer (PBL) not only for the oft-studied convective PBL but more recently for the stable PBL. Thus far, the SBL studies have been aimed mostly at weakly stable boundary layers over horizontally homogeneous surfaces. In addition, the LES velocity fields have been used to simulate dispersion in these PBL flows by tracking "passive" particles using a Lagrangian particle dispersion model (LPDM).

Under previous support from the Army Research Office (ARO), we developed LPDMs for dispersion in convective and stable PBLs including some with a forest canopy and showed that predicted concentration fields agreed well with laboratory data and field observations (*e.g., Weil et al.*, 2004, 2006, 2012). For the ARO program just completed, we extended the previous effort to investigate dispersion in more stable PBLs and SBLs over horizontally heterogeneous surfaces. This effort was pursued in part using our new coupled multi-layer canopy - soil model (*Patton et al.*, 2008). The program consisted of three main investigations. The first (Section 2) had two parts: a) further development of the coupled-canopy LES and comparison with observations from the CHATS (Canopy Horizontal Array Turbulence Study) field program (*Patton et al.*, 2011), and b) modeling of canopy dispersion using the LPDM-LES approach and assessment of the modeled dispersion against the observed CHATS dispersion data. The second (Section 3) investigation targeted the effects of surface temperature heterogeneity on dispersion in the SBL. The third study a) used the coupled model to produce a more stable boundary layer and applied the LES fields generated from this to drive our LPDM (Section 2), and b) developed an LPDM based on parameterized turbulence profiles for modeling dispersion in more stable PBLs (Section 4).

2. Coupled-Canopy LES of the PBL and Dispersion Modeling

2.1 Coupled-Canopy LES and CHATS Meteorological Data Analysis

Under earlier ARO funding, we developed a coupled canopy-soil model by extending the NOAH land-surface system to include a vertical distribution of the sensible-, radiative-, and latent-heat fluxes, a height-dependent leaf-area density, stomatal resistance and leaf boundary layer resistances. This new land-surface model is suitable for coupling with either one-dimensional models of canopy turbulence and scalar transport that could be implemented in mesoscale models, or with turbulence resolving simulations like those generated by large-eddy simulation (Fig. 1). The intent is to allow for dynamic calculation of vegetation-imposed scalar sources/sinks determined by atmospheric demand, and to provide an avenue for the fluid mechanics to respond to rapidly-fluctuating leaf temperatures. Under our current funding, this canopy-resolving land-surface model has been coupled to NCAR's large-eddy simulation code. This coupled modeling system serves as the basis for generating the canopy-influenced wind fields in our CHATS-focused investigations of stability influences on contaminant

Table 1: *Bulk parameters characterizing the two LES cases, LES-WS: $U_g = 8\ ms^{-1}$, and LES-S: $U_g = 4\ ms^{-1}$. The quantities presented are: 1) the friction velocity at canopy top h, where $u_* = (\langle u'w'\rangle^2 + \langle v'w'\rangle^2)^{1/4}$, 2) the PBL depth, z_i defined as the height of the maximum vertical gradient in virtual potential temperature above the canopy, 3) the Monin-Obukhov length evaluated at canopy top, $L = -u_*^3/(k\,[g/\langle\theta_v\rangle]\,\langle w'\theta_v'\rangle)$, and 4) the bulk Richardson number $R_{i_B} = ([g/\langle\theta_v\rangle]\,\Delta\theta_v\,\Delta z)/([\Delta\langle u\rangle]^2 + [\Delta\langle v\rangle]^2)$ evaluated over two different height ranges Δz; from $0 \leq z \leq h$ and from $h \leq z \leq z_i$.*

	u_* (ms^{-1})	z_i (m)	L (m)	h/L	z_i/L	R_{i_B} $0 \leq z \leq h$	R_{i_B} $h \leq z \leq z_i$
LES-WS	0.29	172	204	0.05	0.85	0.02	0.13
LES-S	0.08	106	12	0.85	9.01	1.39	0.31
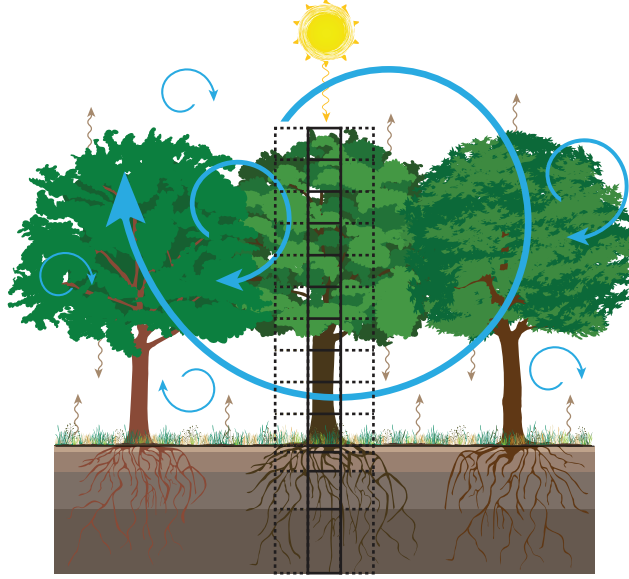
Figure 1: *A schematic depicting the vertically-resolved one-dimensional coupled canopy model (solid black lines). The vertical distribution of canopy density and associated percentage of each grid volume occupied by sunlit versus shaded leaves and their scattering/absorbing efficiency for photosynthetically active and near-infrared radiation is prescribed. In addition, soil moisture and temperature profiles and incoming solar radiation are imposed. At each atmospheric grid volume resolving the vegetation, a leaf-energy balance is solved for sunlit and shaded leaves based upon the total radiation absorbed (assuming a random distribution of nine different leaf angles for scattering and absorbing direct and diffuse radiation) and the local atmospheric winds, temperature, and moisture. The exchange of water vapor and heat between the leaves and the surrounding atmosphere is therefore controlled through a balance of atmospheric demand, photosynthesis, and soil water availability to the trees roots through boundary layer and stomatal conductances for moisture and heat. In the turbulence-resolving large eddy simulation code, a separate implementation of this 1D canopy-resolving land-surface model resides at each horizontal grid point and extends vertically from the surface into the atmosphere up to canopy top. Currently, ten grid points resolve the 10m-tall canopy and four grid points resolve the 1m-deep soil.*

dispersion.

Under Task 1a, simulations using the coupled LES-canopy system have been used to investigate stably stratified canopy turbulence. These simulations used $512 \times 512 \times 256$ grid points to resolve a $512 \times 512 \times 256$ m^3 domain. The simulations were generated by initiating the calculations with weak solar forcing and allowing the sun to set. As the solar forcing diminishes, the coupled canopy slowly cools and subsequently cools the atmosphere in contact with it. Two different stabilities were generated by modifying the geostrophic wind (U_g), where $U_g = 4$ or 8 ms^{-1}. Table 1 presents bulk parameters more fully characterizing the simulations.

Task 1a also focused on evaluating the coupled canopy model across a wide range of atmospheric stability and establishing the mechanisms responsible for turbulent exchange between the canopy layers and those aloft with increasing importance of buoyancy forces. Towards that end, data analysis of the CHATS 30-m meteorological tower was performed (*Dupont and Patton*, 2012a,b) to investigate the variation of velocity, temperature, and humidity fields and their statistical properties with atmospheric stability and seasonal canopy changes, and the mechanisms leading to momentum/scalar transport. This CHATS data analysis serves to evaluate the simulations.

The CHATS meteorological high-rate data from the 30-m tower revealed the sensitivity of velocity, temperature and humidity fields within and above the walnut canopy to atmospheric stability and seasonal canopy changes (*Dupont and Patton*, 2012a,b). This analysis was performed both prior to and following leaf-out of the trees and hence resulted in both de-foliated and foliated periods. Profiles of meteorological statistical properties were analyzed for five stability regimes and two seasonal periods. In addition, an analysis in terms of flow structures within and above the canopy was made to highlight the flow character using the well-established mixing-layer analogy (*Finnigan*, 2000; *Finnigan et al.*, 2009). In near-neutral conditions, the canopy flow better resembles a
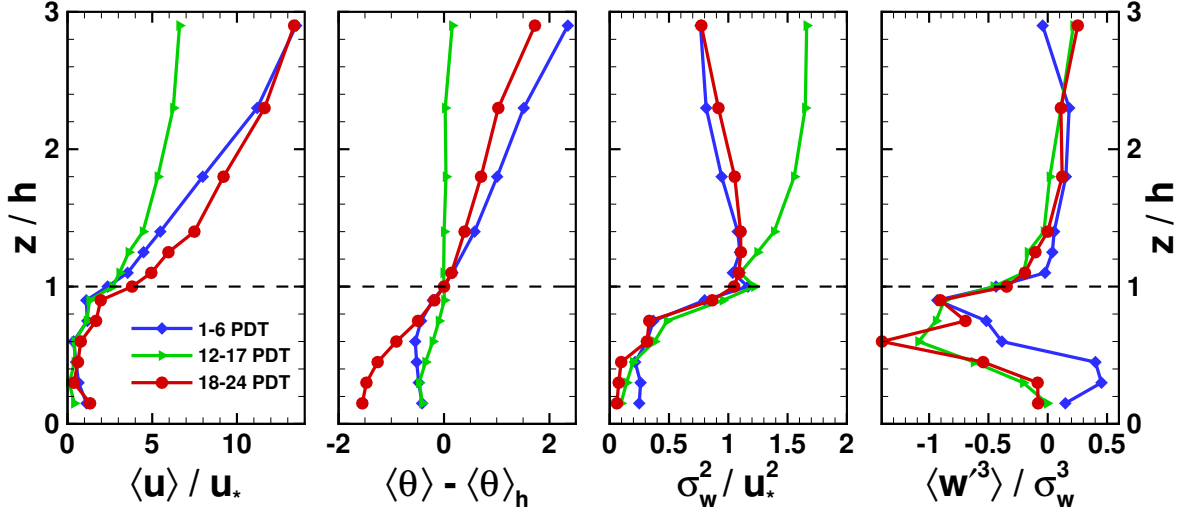
Figure 2: *Vertical profiles of the mean wind normalized by the friction velocity at canopy top $\langle u \rangle / u_*$ (left), potential temperature minus the canopy-top potential temperature in Kelvin (middle-left), vertical velocity variance normalized by u_*^2 (middle-right), and vertical velocity skewness (right) during CHATS when there were leaves on the trees. The profiles are created by averaging over the same time-periods during which the dispersion experiments took place, which are 1-6 PDT, 12-17 PDT, and 18-24 PDT on June 9, 2007. The dashed line represents the top of the canopy, $z/h = 1$.*
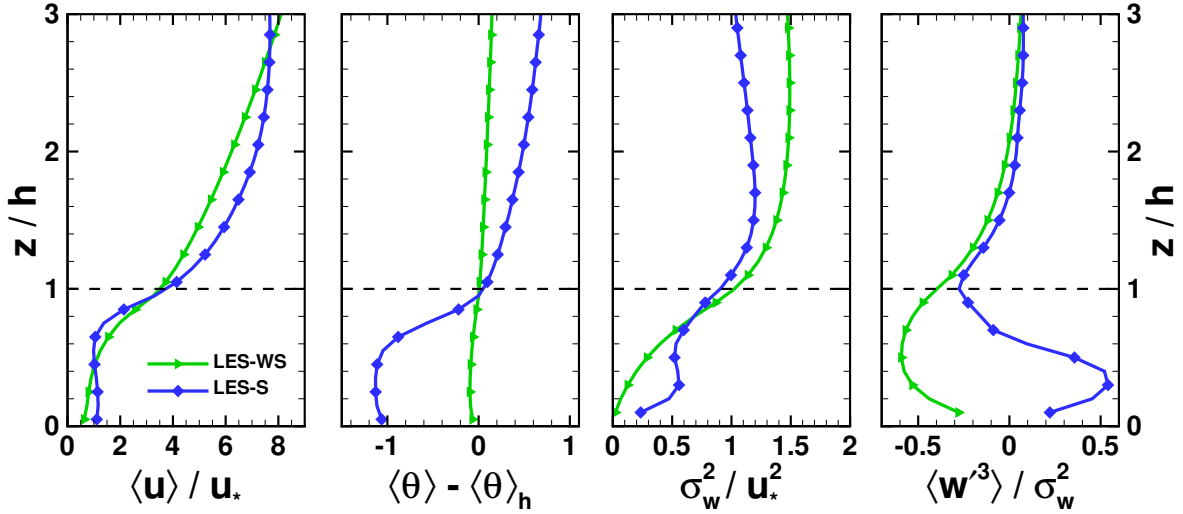
Figure 3: *Horizontally- and time-averaged vertical profiles of the mean wind normalized by the friction velocity at canopy top $\langle u \rangle / u_*$ (left), potential temperature minus the canopy-top potential temperature in Kelvin (middle-left), vertical velocity variance normalized by u_*^2 (middle-right), and vertical velocity skewness (right) from the coupled-canopy turbulence-resolving large eddy simulations mimicking the periods during CHATS when the dispersion experiments took place. The profiles are calculated from two nearly identical simulations that only vary in the geostrophic wind driving the flow; $U_g = (8, 4)$ ms^{-1} for cases (LES-WS, LES-S), respectively, where these geostrophic wind variations result in two different stability conditions: weakly stable (LES-WS) and stable (LES-S). Note that the axis-ranges differ slightly between Figures 2 and 3.*
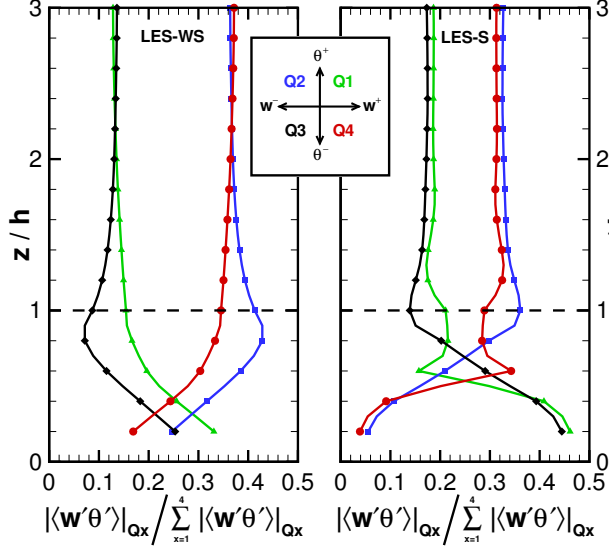
Figure 4: *Horizontally- and time-averaged vertical profiles of the percentage of the heat flux $\langle w'\theta'\rangle$ taking place in each of the four quadrants (Q1-Q4, see inset) for the two LES cases; LES-WS (left) and LES-S (right). Note that for any variable χ: χ^+ signifies $\chi' > 0$, and χ^- signifies $\chi' < 0$.*

plane mixing-layer during the foliated period than in the defoliated period, whereas in the no-leaf period the flow appears more as the superposition of a wall boundary-layer (*e.g.,* over a flat plate) and a plane mixing-layer flow. The plane mixing-layer analogy weakens with deviations from near-neutral stability, whether unstable or stable. For example, in unstable conditions the importance of mixing-layer type structures in the canopy decreases as exhibited by weaker canopy-induced shear of streamwise velocity, lower velocity skewness and kurtosis maxima, and reduced efficiency of the turbulent transport of momentum. In addition, with greater instability, heat and momentum appear to be transported by canopy-scale thermal plumes instead of the mixing-layer type structures.

Figure 2 presents profiles of the mean wind normalized by the canopy-top friction velocity $\langle u\rangle/u_*$, potential temperature deviation $\langle\theta\rangle - \langle\theta\rangle_h$ (in K), dimensionless vertical velocity variance σ_w^2/u_*^2 and vertical velocity skewness $\langle w'^3\rangle/\sigma_w^3$ from CHATS averaged over the five-six hour time periods on June 9 during which the dispersion experiments took place (1-6, 12-17, 18-24) PDT. The simulated mean wind profiles under stable conditions (Fig. 3) exhibit shapes similar to those observed at CHATS (Fig. 2). Like those at CHATS, the stably-stratified simulations reveal significant variation across stability regimes, where the weak wind case develops strong stratification across the canopy top (middle panel, Fig. 3) and the horizontal winds diminish in the subcanopy due to decoupling with the overlying flow. The potential temperature profile for the strongly stable case (middle panel) also mimics the CHATS profiles for similar stability; the temperature inversion near the canopy top is important in limiting the vertical dispersion of scalars emitted within the canopy. Another significant feature is the sign change of the vertical velocity skewness with increasing stability; a feature also found in the CHATS data (Fig. 2). This positive within-canopy vertical velocity skewness indicates that vertical motions in the subcanopy are dominated by small-scale within-canopy buoyant plumes rather than by canopy-induced mixing-layer eddies and has significant implications for canopy dispersion.

Quadrant analysis of scalar fluxes decomposes the flux into quadrants based upon the sign of the fluctuating quantities contributing to the co-variance (*e.g., Willmarth and Lu*, 1972) and helps quantify the character of the turbulent motions performing the transport. Fig. 4 presents a quadrant analysis based upon horizontal- and time-averages of the two stably-stratified large eddy simulations. It is important to note that Fig. 4 presents the quadrant analysis in magnitude fraction form (*i.e.,* the absolute value of the flux in a particular quadrant normalized by the sum of the absolute value of the flux across all four quadrants) which eliminates the sign of the flux and forces the sum over all four quadrants to a value of one.

For weakly stable conditions (LES-WS, left panel Fig. 4), the majority of the flux occurs in quadrants Q2 (downward moving warm air) and Q4 (upward moving cool air), with Q2 becoming increasingly important in the canopy's vicinity (*i.e.,* , below $z/h = 2$). This heat flux partitioning is consistent with organized turbulent

motions generated by velocity shear at the canopy-top transporting warm air downward into the canopy from aloft penetrating nearly to the ground surface with slightly weaker importance of cool within-canopy air transported upwards out of the canopy (*e.g., Chen*, 1990; *Katul et al.*, 1997; *Thomas and Foken*, 2007). With increasing stability (LES-S, right panel Fig. 4), Q2 and Q4 events still dominate transport in the upper canopy and above, but do not reveal as significant an increase in Q2 events with descent toward the canopy top compared to LES-WS. Deep in the canopy ($z/h \le \sim 0.6$), relatively warm soils beneath the relatively cool canopy-top air generates vertical motions such that these layers are dominated by upward moving warm air (Q1) and downward moving cool air (Q3). The leaves in the canopy's upper reaches are exposed to the sky in both simulations, however in LES-S, these leaves radiatively cool more quickly than the rate at which warm air is transported downward from aloft creating the relatively strong stratification occurring at $z/h = \sim 0.8$ (Fig. 3, second panel). This strongly stratified layer acts like a barrier to vertical transport, thereby suggesting that the shear-generated eddies at canopy-top do not (or infrequently) penetrate all the way to the surface; a feature significantly impacting the escape efficiency and/or vertical exchange of contaminants emitted within the canopy's lower levels.

### 2.2 CHATS Dispersion Data Analysis and LPDM-LES Modeling

The main purpose of the CHATS dispersion experiment was to determine the effects of canopy-induced stability on vertical dispersion, especially at night when air in the lower canopy was unstable but air in the upper canopy and above it was stable. This was intended to fill a void in canopy dispersion experiments, *i.e.,* most canopy dispersion experiments have been conducted during near-neutral conditions. For the 6-day experiment, there were two daytime periods (of about 4 - 6 hours duration) and five nighttime periods of a similar duration. In the experiment, an SF_6 tracer was released from a 100-m long line source in the 10-m deep walnut orchard; the source was located 40 m upwind of the 30-m tall meteorological tower and was elevated about a meter above the surface. The key ambient measurements were SF_6 concentrations obtained from seven heights on the tower and nine ground-level SF_6 samplers located at distances of 20 m to 120 m from the source.

Stability effects on dispersion over the diurnal cycle were well-demonstrated by vertical profiles of the hourly-averaged SF_6 from the 30-m tower. During daytime (Fig. 5a), the observations showed that the concentration decreased upwards, often with a concave upwards shape, which is typical of a surface release in an unstable or convective boundary layer. In Fig. 5a, the above-canopy stability ranged from weakly unstable (early afternoon) to weakly stable in the late afternoon, while exhibiting weak (stability, instability) in the (upper, lower) canopy layers, respectively. However, at night the profiles exhibited much higher surface concentrations and a more rapid decrease with height at least for the higher wind cases before midnight (Fig. 5b). The kink in the SF_6 profile ($z = 7$ m; Fig. 5b) near the plume top is in middle of an elevated inversion or stable layer in the upper part of the canopy; *e.g.,* see the potential temperature profile for the stable LES case (LES-S) in Fig. 3. Due to the stable stratification, vertical mixing would be suppressed at short travel times or distances (*i.e.,* $x = 40$ m, Fig. 5) but exhibit a more gradual height variation further downstream as shown in Fig. 8.

In the weak and variable winds after midnight and in the early morning ($U_h \sim 0.4$ ms^{-1}), the surface concentrations were typically higher and more variable, and the vertical SF_6 profiles tended towards fuller shapes, sometimes concave downwards (Fig. 5c). In this third period, the stability as represented by the vertical potential temperature gradient was not as large as during the pre-midnight period, which may explain the somewhat greater plume depth in Fig. 5c than in Fig. 5b.

In our LPDM approach, we track single particles to obtain the mean dispersion and concentration field. When using LES velocities to drive the model, we divide the particle velocity into "resolved" and "subfilter-scale" (SFS) components, consistent with the LES. The SFS velocity is a random value obtained from a stochastic model using the SFS turbulent kinetic energy. In addition, the LPDM-LES approach can be used to obtain an ensemble of dispersion realizations for determining the mean, root-mean-square deviation, and fluctuating fields of dispersion quantities; this has been done for the convective boundary layer (*Weil et al.*, 2012).

The LES fields for the weakly-stable (LES-WS) and stable (LES-S) simulations discussed in Section 2.1 were used to obtain the LPDM mean concentration fields; about 1.1×10^5 particles were released from the modeled
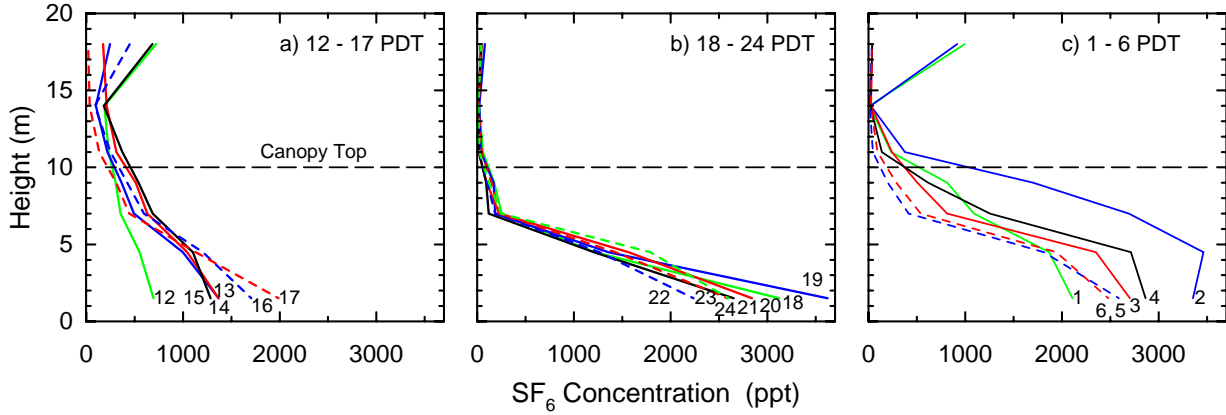
Figure 5: *Vertical profiles of SF$_6$ concentration at $x = 40$ m downstream of a line source showing the diurnal variation of the profiles during CHATS; data are from June 9, 2007 with hour of observation noted next to lines.*

line source in the lower canopy. The LPDM vertical concentration profile is compared with the CHATS SF$_6$ data for the daytime cases (Fig. 6) and has a shape generally similar to the measurements, but underestimates the near-surface concentrations by about 20% on average. This is likely due to the stability differences—modeled versus observed—over the 6-hr period. However, other comparisons (Figs. 7 and 8) with the surface sampler data shows quite good agreement, and thus there is the possibility of small differences between the ground-level and tower measurements.

The surface concentration and its variation with downwind distance is a key quantity of interest. LPDM calculations were made for SBL conditions that approximated but were not identical to the field observations, thus requiring scaling of the results. For similar meteorological conditions, the concentration scaling for a canopy line source of strength Q_ℓ is $CU_h h/Q_\ell = f(X_h)$, where $X_h = u_* x/(U_h h)$ is a dimensionless time or distance, x is the distance from the source, and C is the concentration. The dimensionless concentration versus X_h then should be the same in the model and field and was used to scale the LPDM runs for the LES-WS and LES-S fields to two observational periods: 1) the near-neutral daytime case (Fig. 5a, which for the sake of comparison will be called WS), and 2) the early nighttime case (Fig. 5b, and will be called S). The wind and turbulence fields from LES-WS are good approximations for WS, and those from LES-S are only rough approximations for S.

Figure 7 shows the concentration versus distance for the two periods. For the WS case (green line), the LPDM result agrees well with the observations, and the concentration falls off approximately as $C \propto x^{-1}$ near the source ($x \leq 40$ m), which is consistent with dispersion in a PBL with no canopy (*e.g., van Ulden*, 1978). However, for 40 m $< x <$ 120 m, the concentration decreases more sharply as $C \propto x^{-2}$, which has no counterpart for the PBL without a canopy. This decrease results from both turbulent dispersion and the canopy-induced strong vertical shear of the horizontal wind speed across the canopy top (left panel, Figs. 2 and 3). Over the 40 m to 120 m distance, the mean plume height $\bar{z}_p$ increases from $0.7h$ to $1.5h$ with a distance dependence like $\bar{z}_p \propto x$, and the vertical plume spread σ_z exhibits a similar dependence (not shown). Furthermore, for this height change, the mean wind U increases by a factor of three (Fig. 3), and the mean plume speed varies as $U_p \propto x$. Since the concentration behaves as $C \propto Q_\ell/(U_p \sigma_z)$, $U_p(x)$ provides for additional dilution of the plume as shown in Fig. 7, *i.e.,* to produce the $C \propto x^{-2}$ dependence. For greater distances (*i.e., $x >$ 120 m*), the concentration tends towards a $C \propto x^{-1/2}$ variation, which is consistent with the long-time concentration behavior in a PBL with no canopy.

The LPDM results for the stable (S) case, scaled to the conditions for the nighttime period in Fig. 5b, are given by the blue lines in Fig. 7. Due to the very weak canopy-top winds ($U_h = 0.48$ ms^{-1} in the LES), the LPDM mean concentration field is developing with time, and results are shown for two emission time durations, 38 min and 64 min, with the latter exhibiting high concentrations extending further downwind. This trend of increasing concentration with distance and time is expected to continue, thus requiring longer-time simulations. Nevertheless, the S case (64 min) exhibits higher concentrations than the WS case as would be expected, and the
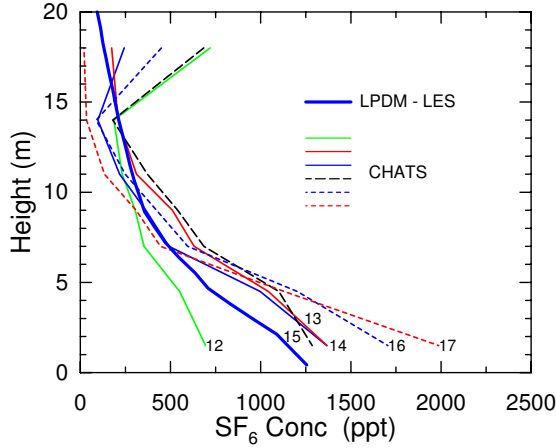
Figure 6: *LPDM and observed vertical profiles of SF$_6$ concentration downstream of a line source during daytime in CHATS; data from June 9, 2007.*
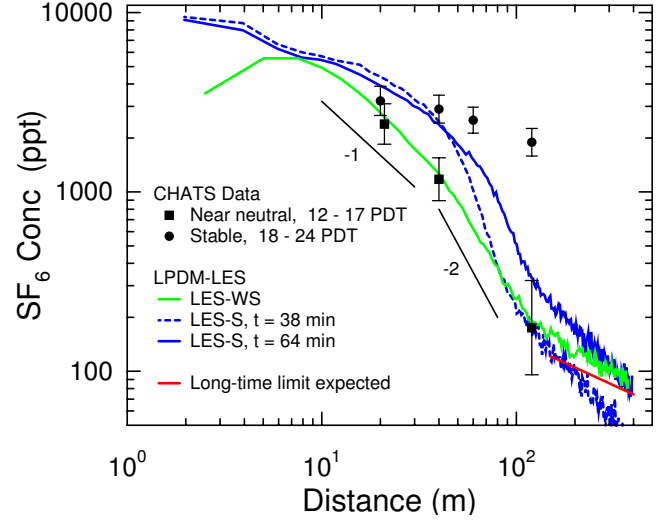
**Figure 7:** *LPDM and observed SF$_6$ surface concentration as a function of distance downwind of a line source during CHATS on June 9, 2007. Points and error bars show the mean and root-mean-square deviation in concentration over each measurement period.*

model results agree approximately with the observations at very short range, $x \leq 40$ m. We believe that model predictions for longer emission times would approximate better the measurements at greater distances.

Figure 8 shows the modeled time or distance evolution of the vertical profiles of concentration for the two LPDM-LES cases and the important differences between them. The LPDM-LES results from the LES-WS case exhibit a "lapse" or continuously decreasing vertical gradient of the dimensionless concentration with z/h and X_h as a result of the weakly-stable stratification within and above the canopy. In contrast, LPDM-LES results using data from the LES-S case leads to an elevated within-canopy scalar concentration inversion with approximately uniform (or slightly increasing) values below the inversion; the uniform value results from the weak convection and turbulence below the inversion (Fig. 3) which generate vertical mixing driven by the contrast between the relatively warm soil and the leaf-induced cool air in the upper canopy. Essentially, the plume mimics the thermal structure but the scalar inversion strength continually decreases with X_h due to the: 1) small "line" nature and dimension of the scalar source versus the larger areal nature of the thermal source, and 2) the stronger wind and turbulence above the canopy-induced inversion which "mixes out" the scalar from the canopy and decreases its inversion strength with increasing time or X_h.

3. Surface Temperature Heterogeneity Effects on Dispersion in the SBL

This study follows previous work by *Stoll and Porte-Agel* (2009) and *Mironov and Sullivan* (2010) who showed how the surface-temperature heterogeneity modified the SBL structure and turbulent transport properties relative to a surface-temperature homogeneous SBL. Both boundary layers were cases of a weakly stable boundary layer (WSBL) with moderate-to-strong winds. In *Mironov and Sullivan* (2010), the temperature heterogeneity was generated with spanwise homogeneous surface temperature strips that had a sinusoidal variation in the x (mean wind $\langle u \rangle$) direction and a horizontal-mean surface temperature that was the same as in the homogeneous SBL. Both studies showed that the heterogeneous (HET) SBL was more turbulent and well-mixed with respect to temperature than the homogeneous (HOM) SBL. An outstanding finding from *Mironov and Sullivan* (2010) was that the temperature variance peaked both at the surface and at the SBL-top with maximum values far greater than in the HOM case. Throughout the bulk of the HET SBL, the temperature variance was relatively uniform or "well-mixed" which contrasted with the more vertically-inhomogeneous structure of the HOM SBL.

11
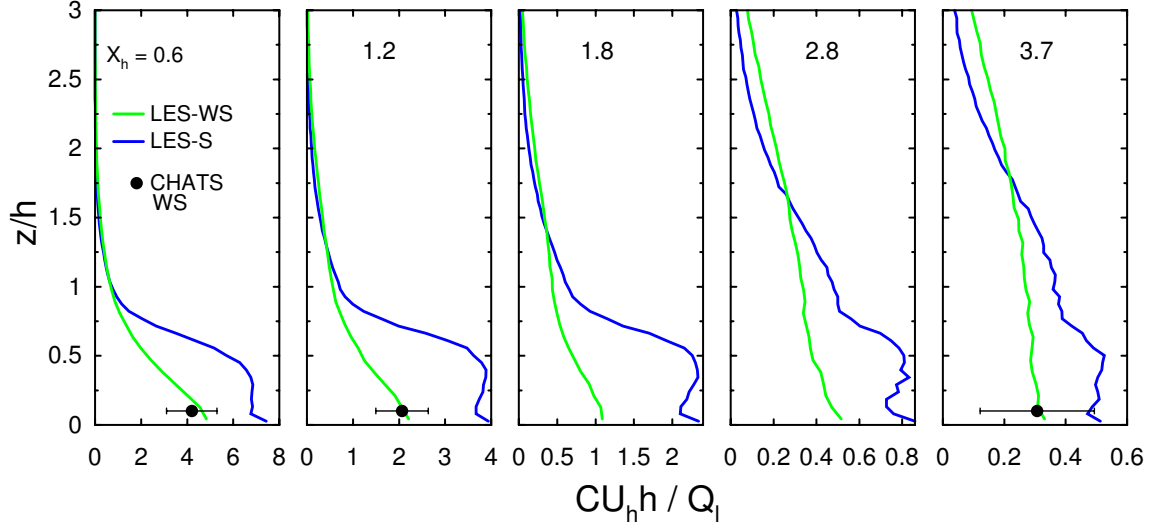
Figure 8: *Evolution of LPDM vertical profiles of the dimensionless concentration with dimensionless distance X_h downstream of a line source in weakly-stable (WS) and stable (S) boundary layers. LPDM WS results compared with CHATS surface-sampler data for daytime (hours 12 - 17 on June 9, 2007); points and error bars have definition as in Fig. 7.*

We used the LES fields from *Mironov and Sullivan* (2010) to drive the LPDM and investigate the dispersion characteristics for a continuous source at different heights in the two SBLs. Heterogeneity effects can be assessed by comparison to our earlier results for the homogeneous SBL (*Weil et al.*, 2006). This comparison was simplified since the LES fields in the *Mironov and Sullivan* (2010) work were created for the same domain size [$(400 \text{ m})^3$], number of grid points ($200 \times 200 \times 192$), geostrophic wind U_g ($= 8 \text{ ms}^{-1}$), initial stratification, and other conditions as for the HOM SBL described in *Weil et al.* (2006). For the HET SBL, the $z_i = 221$ m, $u_* = 0.27 \text{ ms}^{-1}$, and the vertically-averaged wind speed U was 7.4 ms^{-1}, which are all close to their counterparts for the HOM case.

We conducted LPDM simulations for several source heights, but our main focus was on a surface release in order to explain the large surface temperature variance found by *Mironov and Sullivan* (2010). Calculations were made for sources at the leading edge of the hot and cold strips and in the middle of each strip, where the strip length in the *x* direction was 200 m; hence, sources were located at $x_s = 0$, 100, 200, and 300 m along the *x* axis with about 17 sources spanning the strip in the *y* direction. For each *y*-strip of sources, 10 realizations of the concentration field were obtained using a sequence of initialization times that were about 1 min apart, and 1.28×10^5 particles were released in each realization.

Our results showed an oscillatory behavior of the mean concentrations with distance downwind of the source. This was attributed to the sinusoidally-varying surface temperature which generated gravity waves in this stratified flow. An understanding of this behavior can be made with reference to the *Sullivan and McWilliams* (2002) study of turbulent flow over water waves in the presence of stable stratification, where the surface waves generated gravity waves in the air above the water. Following their analysis, we decomposed the instantaneous concentration c as $c(x,y,z,t) = C(x,y,z) + c_w(x,z) + c'(x,y,z,t)$, where C is the ensemble-mean concentration, c_w is a phase-averaged concentration, c' is a turbulent fluctuation, and x, y, z are measured with respect to the source location. The ensemble-mean concentration for a particular line or strip of sources (along y at a fixed x_s) is $\langle c \rangle = C + c_w$, where $\langle \rangle$ denotes an ensemble average. Our focus is on C and c_w.

The mean concentration C was obtained by averaging the concentrations from a large number (289) of sources evenly distributed over the LES *x-y* domain as in *Weil et al.* (2004). Here, we analyze the crosswind-integrated concentration (CWIC) C^y nondimensionalized as $C^y U z_i/Q$ as a function of the dimensionless distance $X = u_* x/(U z_i)$, where Q is the source strength. The LPDM surface CWIC results for the HET and HOM SBLs
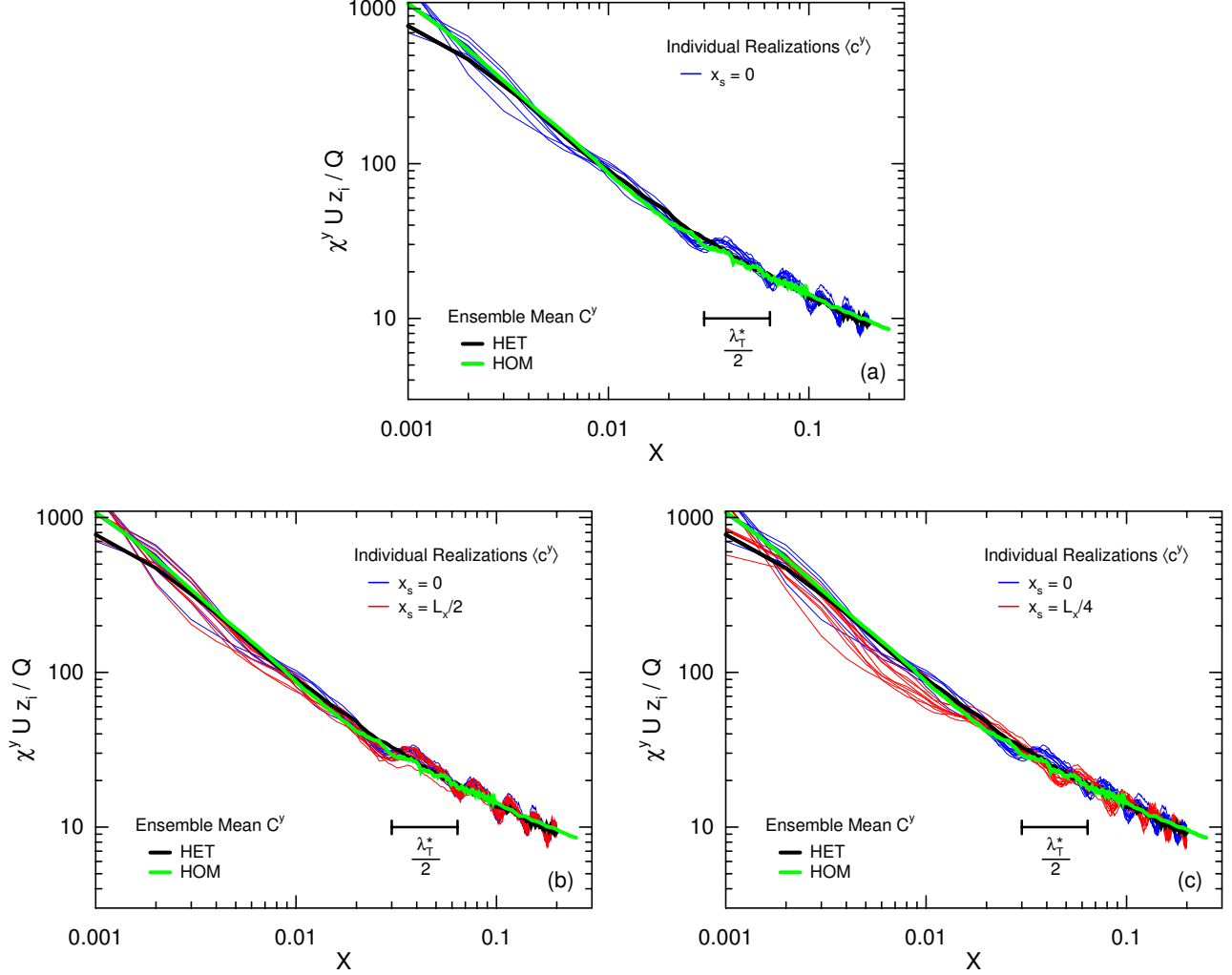
Figure 9: *Dimensionless crosswind-integrated integrated concentration (CWIC) at the surface as a function of dimensionless distance due to a surface source in a surface-temperature heterogeneous SBL: a) source ($x_s = 0$) at leading edge of hot strip, b) source ($x_s = L_x/2$) at leading edge of cold strip, and c) source ($x_s = L_x/4$) in middle of hot strip. χ^y denotes either the mean CWIC C^y or the average CWIC over a y-strip of sources at fixed x_s, i.e., $\langle c^y \rangle$. Ensemble-mean CWIC from the heterogeneous and homogeneous SBLs shown for reference. Here, $\lambda_T^* = \frac{u_* \lambda_T}{U z_i}$ and $\lambda_T = L_x$.*

were in excellent agreement with one another as shown in Fig. 9. This assures one of the similarity in the vertical structure of the mean wind and turbulent velocity statistics in these two SBLs; these variables drive the mean dispersion. The mean CWIC results also agree well with field observations (not shown) from the Prairie Grass experiments (*Barad*, 1958).

Figure 9a also shows the mean dimensionless CWIC $\langle c^y \rangle$ versus X for sources at the leading edge of the hot strip ($x_s = 0$). The $\langle c^y \rangle$ is the average of the 10 realizations, which do not exhibit a large scatter, and only the realizations are shown; the actual average will be presented in the future. As is clear, the $\langle c^y \rangle$ oscillates over the entire distance range shown which is about three times the domain length $L_x = 400$ m or $X_L = 0.064$ in dimensionless distance (X) units. Note that the $\langle c^y \rangle$ oscillates with a wavelength λ_w that is about half of the surface temperature wavelength λ_T, i.e., $\lambda_w = \lambda_T/2$. The shorter wavelength for the c_w can be explained by reference to the *Sullivan and McWilliams* (2002) study, which showed that the wave-induced heat flux $\theta_w w_w$ generated by the water waves had a wavelength one-half of the water surface wavelength. This occurred because the wave-induced temperature (θ_w) and vertical velocity (w_w) perturbations were 90° out-of-phase. We believe

that the same phenomena exists in this heterogeneous situation and explains the shorter λ_w.

Figure 9b shows similar results (red lines) for sources located along the leading edge of the hot strip ($x_s = L_x/2 = 200$ m) and overlaid on those (blue lines) from Fig. 9a. The averages or $\langle c^y \rangle$ versus X from these two sources are in-phase, which further supports the shorter wavelength λ_w for the c_w field. Finally, Fig. 9c presents results for a source at the midpoint of the hot strip ($x_s = L_x/4$), and shows that the $\langle c^y \rangle$ is 90° out-of-phase with the results for $x_s = 0$.

The net result for c^y from a distribution of surface sources over the $x - y$ domain of a HET SBL is that the ensemble-mean C^y concentration would be similar to the HOM SBL as shown above, but the variance would not. The variance would contain a $c_w^2(x,z)$ term applicable at distance x downwind of a particular source, and for a distribution of sources, these variance terms would be superposed to produce a total variance greater than the that due to the SBL turbulence alone, *i.e.,* $\langle c'^2 \rangle$. In the HET SBL analyzed by *Mironov and Sullivan* (2010), the temperature variance was quite large implying a non-negligible contribution from c_w or θ_w due to the surface temperature distribution.

4. A Parameterized LPDM for Moderate to Very Stable Boundary Layers

This study aimed at the development of a relatively simple model for understanding and predicting the behavior of the mean wind, potential temperature, and flux profile behavior in the SBL over a broad range of stability—from a weakly-stable (WSBL) to a very-stable (VSBL) boundary layer. The model was based on the equations governing the above variables and used an eddy-diffusivity (K) closure from the *Brost and Wyngaard* (1978) model. This was intended to provide some preliminary information for moderately- to very-stable PBLs, where LES currently does not. The modeled or parameterized profiles of the mean wind, temperature, and turbulence for these more stable cases can be and have been used to drive an LPDM for dispersion predictions in these conditions. We label this the LPDM-PT, which is based on parameterized turbulence (PT) and winds.

An eddy-diffusivity (K) approach is justified for modeling the mean wind, temperature, etc. in the SBL because of the small turbulence length scales in the SBL as found from field data and LES. In addition to use of the *Brost and Wyngaard* (1978) K profiles, there are two other important aspects of this "K-model" approach (*Weil*, 2011): a) reduction of the model equations to a simple ordinary differential form using a similarity variable, and b) modeling of the flux profiles using a simple K approach. The model has been tested in two SBL limits and agrees well with: 1) LES results and field data for a WSBL ($z_i/L = 1.6$), and 2) field observations for a VSBL ($z_i/L = 42$), where z_i and L are the SBL height and Monin-Obukhov length, respectively. Note that in the following figures and discussion, we also use $h = z_i$ to denote the SBL height.

Figure 10 presents the evolution of the modeled temperature difference profiles for a VSBL, $z_i/L = 42$, and compares them with the CASES99 field data (*Mahrt and Vickers*, 2006). The agreement is good and shows that the SBL dimensionless profiles do not change much with time. This is due to the very small diffusivity in the VSBL by comparison to that in the WSBL, where the larger K leads to a greater time variation and different profile shapes.

Figure 11 presents the "K-model" SBL wind profiles for a broad range of stability, where the stability index $z_i/L = 1.6$, 10, and 40. The modeled profiles agree approximately with other results in two comparisons: the LES prediction (dashed blue line) for the WSBL ($z_i/L = 1.6$) and the CASES99 field data for a VSBL ($z_i/L = 42$), which occurred for a weak wind U_h ($\simeq 3$ m/s) at the SBL top. An alternative stability index is the bulk Richardson number Ri_{bh} which is based on the SBL depth, the potential temperature change $\Delta\Theta_h$ over the SBL, and the U_h. For CASES99, the $Ri_{bh} \simeq 1.2$ and is at or near the critical value or limit (*i.e.,* 1) for turbulence to exist or be maintained. A comparison for much weaker winds ($U_h \simeq 0.35$ m/s) in the FLOSS experiment (*Mahrt and Vickers*, 2006) showed that the model did not work well for the wind and flux profiles; here, the Ri_{bh} was 51 and hence much greater than 1. At FLOSS, the U_h was so low that mechanically-forced turbulence was extremely weak and dominated by other forcings, *e.g.,* density-driven flows and turbulence. As a result, we tentatively believe that the "operating range" of the LPDM based on the parameterized winds and turbulence is for $z_i/L \leq 40$ or perhaps
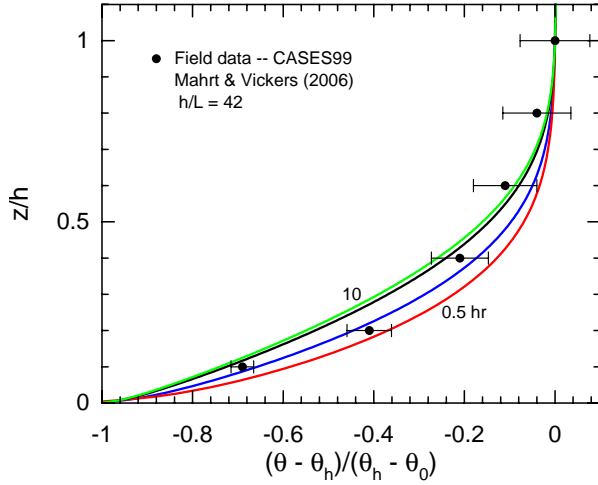
Figure 10: *Profiles of dimensionless potential temperature as a function of time for a VSBL, $z_i/L = 42$; here $h = z_i$, the SBL height.*
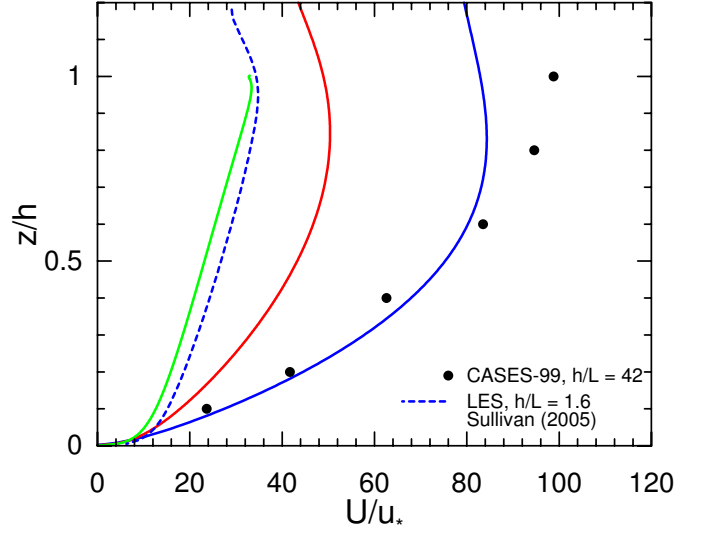
Figure 11: *Mean wind profile in the stable boundary layer from the "K-model" as a function of the stability index h/L for $h/L = 1.6$ (green line), 10 (red line), and 40 (blue line). K-model prediction can be compared with LES result for a WSBL ($h/L = 1.6$) and CASES99 data for a VSBL ($h/L = 42$).*

somewhat larger and/or $Ri_{bh} \leq 1.2$. These limits need further clarification.

For concentration estimates using the LPDM-PT, we could adopt the *K*-model wind profile but have initially chosen a simpler method in which the MO profile is corrected for the stability. The correction is an exponentially-decaying function of z/z_i, $\exp(-\alpha z/z_i)$, where the parameter α is empirically chosen and depends on z_i/L. Figure 12 shows that the corrected MO profile is a good match to the *K*-model profile over most of the SBL. In addition, the LPDM-PT requires the vertical turbulence velocity σ_w. Figure 13 shows a σ_w parameterization (red line) compared with a range of results: a) *Nieuwstadt*'s (1984) field data, LES results, and wind-tunnel data all for a WSBL with $z_i/L \simeq 1.6$, and b) the CASES99 field data for $z_i/L \simeq 42$. We believe that the parameterization is an adequate fit to these diverse results although further work and data are necessary to test or improve the parameterization for more stable conditions, *i.e.,* the VSBL.

Predictions of the crosswind-integrated concentration (CWIC, C^y) due to a surface source in the SBL have been made using the LPDM-PT for a range of stability. The model was compared with surface CWIC observations from the Prairie Grass experiment (*Barad*, 1958), which was conducted over a grass surface and for distances $x \leq$ 800 m. Figures 14 and 15 show the dimensionless CWIC, $C^y U z_i/Q$, as a function of the dimensionless distance X from both the model and experiments for two groups of stability, which range from weakly-to-moderately stable. Although there is a some bias and scatter, the trend and overall agreement between the model and data is considered quite good. Further examination of the Prairie Grass data record and other experiments will be made in an attempt to obtain measurements for more stable conditions, $z_i/L > 5$, for evaluating the model.

5. Summary

This research program extended our previous studies of turbulence and dispersion in the planetary boundary layer (PBL) to more stable PBLs including those interacting with a forest canopy, and to stable boundary layers (SBLs) over horizontally-heterogeneous surfaces. There were four key findings. First, our coupled-canopy large-eddy simulation (LES) model was a) pushed to more stable PBLs than previously achieved with simulation of the vertical structure of mean and turbulence quantities within and above the canopy, including one case producing a 1 K temperature inversion in the upper canopy, and b) verification of this temperature structure by
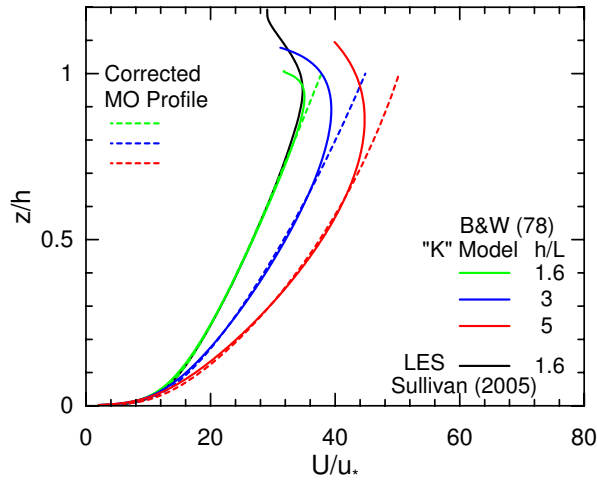
Figure 12: *Comparison between the "corrected" Monin-Obukhov (MO) wind profiles and the K-model profiles in the SBL for weakly- to moderately-stable conditions; here, u_* is the surface friction velocity.*
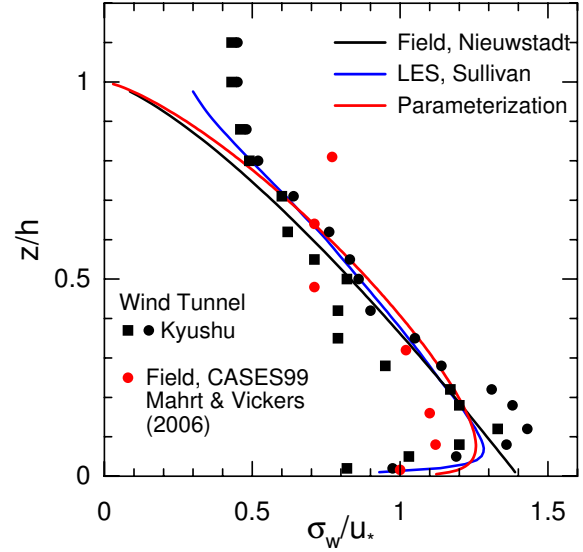

Figure 13: *A parameterization of the dimensionless vertical turbulence component, σ_w/u_*, and comparison with field data, wind-tunnel data, and LES results for a WSBL ($h/L = 1.6$) and CASES99 field observations for a VSBL.*

comparison with field observations in weakly- to strongly-stable conditions in an orchard canopy. Second, the LES fields were used to drive our Lagrangian particle dispersion model (LPDM) for concentration predictions that a) matched observations in the above two stabiliy regimes, b) showed perhaps for the first time the importance of the strong canopy-top wind shear in accelerating the decrease in surface concentrations with downstream distance, and c) produced vertical profiles of scalar concentration that ranged from "lapse" conditions to one with a scalar inversion for strong stability. Third, the LPDM investigations of dispersion in an SBL with either a heterogeneous or homogeneous surface-temperature distribution showed important effects of the heterogeneity. Although the mean concentrations in the HET and HOM cases were similar, heterogeneity can produce signficant surface concentration variance resulting from heterogeneity-induced gravity wave-induced scalar flux; this finding has the potential for determining or identifying the degree of surface-temperature heterogeneity in the SBL from in-situ measurements, satellite observations, and modeling. Fourth, modeled or parameterized profiles of wind, temperature, and turbulence were derived for weakly- to very-stable PBLs and provide the inputs for driving an LPDM based on parameterized turbulence (PT) for stronger stratification. The LPDM-PT was found to give predictions of surface concentrations that matched observations in weakly- to moderately-stable PBLs.

References

Barad, M. L. (1958), Project Prairie Grass. A field program in diffusion, *Geophysical Research Paper No. 59, Vols. I and II AFCRF-TR-235*, Air Force Cambridge Research Center, Bedford, MA.

Brost, R. A., and J. C. Wyngaard (1978), A model study of the stably stratified planetary boundary layer, *J. Atmos. Sci.*, *35*, 1427–1440.

Chen, F. (1990), Turbulent characteristics over a rough natural surface. Part I: Turbulent structures, *Boundary-Layer Meteorol.*, *52*, 151–175.

Dupont, S., and E. G. Patton (2012a), Influence of stability and seasonal canopy changes on micrometeorology within and above an orchard canopy: The CHATS experiment, *Agric. For. Meteorol.*, *157*, 11–29.
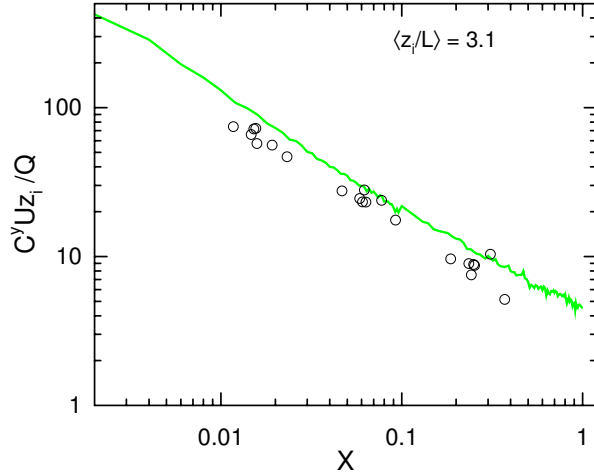
Figure 14: *Dimensionless crosswind-integrated concentration at the surface versus dimensionless downwind distance X for a surface release in the SBL for $z_i/L = 3.1$. In the dimensionless CWIC, Q is the source strength, and $X = u_* x/(U z_i)$, where x is the distance from the source, and U is the mean wind in the SBL. The modeled CWIC from the LPDM-PT (line) can be compared with Prairie Grass observations (points).*
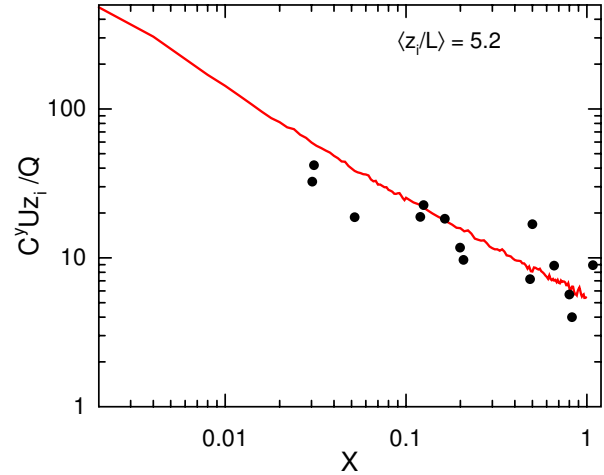
Figure 15: *Same as Fig. 14 but for $z_i/L = 5.2$.*

Dupont, S., and E. G. Patton (2012b), Momentum and scalar transport within a vegetation canopy following atmospheric stability and seasonal canopy changes: The CHATS experiment, *Atmos. Chem. Phys.*, *12*, 5913–5935.

Finnigan, J. J. (2000), Turbulence in plant canopies, *Ann. Rev. Fluid Mech.*, *32*, 519–571.

Finnigan, J. J., R. H. Shaw, and E. G. Patton (2009), Turbulence structure above a vegetation canopy, *J. Fluid Mech.*, *637*, 387–424.

Katul, G., C.-I. Hsieh, G. Kuhn, and D. Ellsworth (1997), Turbulent eddy motion at the forest-atmosphere interface, *J. Geophys. Res.*, *102*(D12), 13,409–13,421.

Mahrt, L., and D. Vickers (2006), Extremely weak mixing in stable conditions, *Boundary-Layer Meteorol.*, *119*, 19–39.

Mironov, D. V., and P. P. Sullivan (2010), Effect of horizontal surface temperature heterogeneity on turbulent mixing in the stably stratified atmospheric boundary layer, in *19th Symposium on Boundary Layers and Turbulence*, Paper 6.3, Keystone, CO.

Nieuwstadt, F. T. M. (1984), The turbulent structure of the stable nocturnal boundary layer, *J. Atmos. Sci.*, *41*, 2202–2216.

Patton, E. G., J. C. Weil, and P. P. Sullivan (2008), A coupled canopy-soil model for the simulation of atmospheric turbulence modified by tall vegetation, in *18th Symposium on Boundary Layers and Turbulence*, 9A.3, Stockholm, Sweden, http://ams.confex.com/ams/pdfpapers/140168.pdf.

Patton, E. G., et al. (2011), The canopy horizontal array turbulence study, *Bull. Amer. Meteorol. Soc.*, *92*, 593–611.

Stoll, R., and F. Porte-Agel (2009), Surface heterogeneity effects on regional-scale fluxes in stable boundary layers: surface temperature transitions, *J. Atmos. Sci.*, *66*, 412–431.

Sullivan, P. P., and J. C. McWilliams (2002), Turbulent flow over water waves in the presence of stratification, *Phys. Fluids*, *14*, 1182–1195.

Thomas, C., and T. Foken (2007), Flux contribution of coherent structures and its implications for the exchange of energy and matter in a tall spruce canopy, *Boundary-Layer Meteorol.*, *123*(2), 317–337, doi: 10.1007/s10546-006-9144-7.

van Ulden, A. A. P. (1978), Simple estimates for vertical diffusion from sources near the ground, *Atmos. Environ.*, *12*, 2125–2129.

Weil, J. C. (2011), Stable boundary layer modeling for air quality applications, in *Air Pollution Modeling and Its Application XXI*, edited by D. G. Steyn and S. T. Castelli, pp. 57–61, Springer.

Weil, J. C., P. P. Sullivan, and C.-H. Moeng (2004), The use of large-eddy simulations in Lagrangian particle dispersion models, *J. Atmos. Sci.*, *61*, 2877–2887.

Weil, J. C., E. G. Patton, and P. P. Sullivan (2006), Lagrangian modeling of dispersion in the stable boundary layer, in *17th Symposium on Boundary Layers and Turbulence*, Paper J6.12, San Diego, CA, http://ams.confex.com/ams/pdfpapers/110925.pdf.

Weil, J. C., P. P. Sullivan, E. G. Patton, and C.-H. Moeng (2012), Statistical variability of dispersion in the convective boundary layer: Ensembles of simulations and observations, *Boundary-Layer Meteorol.*, *in press*.

Willmarth, W. W., and S. S. Lu (1972), Structure of the Reynolds stress near the wall, *J. Fluid Mech.*, *55*, 65–92.